

2015

New Measurement of Antineutrino Oscillation with the Full Detector Configuration at Daya Bay

F. P. An

A. B. Balantekin

J. J. Cherwinka

R. D. McKeown

College of William and Mary

Follow this and additional works at: <https://scholarworks.wm.edu/aspubs>

Recommended Citation

An, F. P., Balantekin, A. B., Band, H., Bishai, M., Blyth, S., Butorov, I., ... & Chang, J. F. (2015). New measurement of antineutrino oscillation with the full detector configuration at Daya Bay. *Physical review letters*, 115(11), 111802.

This Article is brought to you for free and open access by the Arts and Sciences at W&M ScholarWorks. It has been accepted for inclusion in Arts & Sciences Articles by an authorized administrator of W&M ScholarWorks. For more information, please contact scholarworks@wm.edu.



New Measurement of Antineutrino Oscillation with the Full Detector Configuration at Daya Bay

F. P. An,¹ A. B. Balantekin,² H. R. Band,³ M. Bishai,⁴ S. Blyth,^{5,6} I. Butorov,⁷ G. F. Cao,⁸ J. Cao,⁸ W. R. Cen,⁸ Y. L. Chan,⁹
 J. F. Chang,⁸ L. C. Chang,¹⁰ Y. Chang,⁶ H. S. Chen,⁸ Q. Y. Chen,¹¹ S. M. Chen,¹² Y. X. Chen,¹³ Y. Chen,¹⁴ J. H. Cheng,¹⁰
 J. Cheng,¹¹ Y. P. Cheng,⁸ J. J. Cherwinka,² M. C. Chu,⁹ J. P. Cummings,¹⁵ J. de Arcos,¹⁶ Z. Y. Deng,⁸ X. F. Ding,⁸
 Y. Y. Ding,⁸ M. V. Diwan,⁴ E. Draeger,¹⁶ D. A. Dwyer,¹⁷ W. R. Edwards,^{27,17} S. R. Ely,¹⁸ R. Gill,⁴ M. Gonchar,⁷
 G. H. Gong,¹² H. Gong,¹² M. Grassi,⁸ W. Q. Gu,¹⁹ M. Y. Guan,⁸ L. Guo,¹² X. H. Guo,²⁰ R. W. Hackenburg,⁴ R. Han,¹³
 S. Hans,⁴ M. He,⁸ K. M. Heeger,³ Y. K. Heng,⁸ A. Higuera,²¹ Y. K. Hor,²² Y. B. Hsiung,⁵ B. Z. Hu,⁵ L. M. Hu,⁴ L. J. Hu,²⁰
 T. Hu,⁸ W. Hu,⁸ E. C. Huang,¹⁸ H. X. Huang,²³ X. T. Huang,¹¹ P. Huber,²² G. Hussain,¹² D. E. Jaffe,⁴ P. Jaffke,²² K. L. Jen,¹⁰
 S. Jetter,⁸ X. P. Ji,^{24,12} X. L. Ji,⁸ J. B. Jiao,¹¹ R. A. Johnson,²⁵ L. Kang,²⁶ S. H. Kettell,⁴ M. Kramer,^{17,27} K. K. Kwan,⁹
 M. W. Kwok,⁹ T. Kwok,²⁸ T. J. Langford,³ K. Lau,²¹ L. Lebanowski,¹² J. Lee,¹⁷ R. T. Lei,²⁶ R. Leitner,²⁹ K. Y. Leung,²⁸
 J. K. C. Leung,²⁸ C. A. Lewis,² D. J. Li,³⁰ F. Li,⁸ G. S. Li,¹⁹ Q. J. Li,⁸ S. C. Li,²⁸ W. D. Li,⁸ X. N. Li,⁸ X. Q. Li,²⁴ Y. F. Li,⁸
 Z. B. Li,³¹ H. Liang,³⁰ C. J. Lin,¹⁷ G. L. Lin,¹⁰ P. Y. Lin,¹⁰ S. K. Lin,²¹ J. J. Ling,^{4,18} J. M. Link,²² L. Littenberg,⁴
 B. R. Littlejohn,^{25,16} D. W. Liu,²¹ H. Liu,²¹ J. L. Liu,¹⁹ J. C. Liu,⁸ S. S. Liu,²⁸ C. Lu,³² H. Q. Lu,⁸ J. S. Lu,⁸ K. B. Luk,^{27,17}
 Q. M. Ma,⁸ X. Y. Ma,⁸ X. B. Ma,¹³ Y. Q. Ma,⁸ D. A. Martinez Caicedo,¹⁶ K. T. McDonald,³² R. D. McKeown,^{33,34}
 Y. Meng,²² I. Mitchell,²¹ J. Monari Kebwaro,³⁵ Y. Nakajima,¹⁷ J. Napolitano,³⁶ D. Naumov,⁷ E. Naumova,⁷ H. Y. Ngai,²⁸
 Z. Ning,⁸ J. P. Ochoa-Ricoux,³⁷ A. Olshevski,⁷ J. Park,²² S. Patton,¹⁷ V. Pec,²⁹ J. C. Peng,¹⁸ L. E. Piilonen,²² L. Pinsky,²¹
 C. S. J. Pun,²⁸ F. Z. Qi,⁸ M. Qi,³⁸ X. Qian,⁴ N. Raper,³⁹ B. Ren,²⁶ J. Ren,²³ R. Rosero,⁴ B. Roskovec,²⁹ X. C. Ruan,²³
 B. B. Shao,¹² H. Steiner,^{27,17} G. X. Sun,⁸ J. L. Sun,⁴⁰ W. Tang,⁴ D. Taychenachev,⁷ H. Themann,⁴ K. V. Tsang,¹⁷ C. E. Tull,¹⁷
 Y. C. Tung,⁵ N. Viaux,³⁷ B. Viren,⁴ V. Vorobel,²⁹ C. H. Wang,⁶ M. Wang,¹¹ N. Y. Wang,²⁰ R. G. Wang,⁸ W. Wang,³¹
 W. W. Wang,³⁸ X. Wang,⁴¹ Y. F. Wang,⁸ Z. Wang,¹² Z. Wang,⁸ Z. M. Wang,⁸ H. Y. Wei,¹² L. J. Wen,⁸ K. Whisnant,⁴²
 C. G. White,¹⁶ L. Whitehead,²¹ T. Wise,² H. L. H. Wong,^{27,17} S. C. F. Wong,^{9,31} E. Worcester,⁴ Q. Wu,¹¹ D. M. Xia,^{8,43}
 J. K. Xia,⁸ X. Xia,¹¹ Z. Z. Xing,⁸ J. Y. Xu,⁹ J. L. Xu,⁸ J. Xu,²⁰ Y. Xu,²⁴ T. Xue,¹² J. Yan,³⁵ C. G. Yang,⁸ L. Yang,²⁶
 M. S. Yang,⁸ M. T. Yang,¹¹ M. Ye,⁸ M. Yeh,⁴ Y. S. Yeh,¹⁰ B. L. Young,⁴² G. Y. Yu,³⁸ Z. Y. Yu,⁸ S. L. Zang,³⁸
 L. Zhan,⁸ C. Zhang,⁴ H. H. Zhang,³¹ J. W. Zhang,⁸ Q. M. Zhang,³⁵ Y. M. Zhang,¹² Y. X. Zhang,⁴⁰ Y. M. Zhang,³¹
 Z. J. Zhang,²⁶ Z. Y. Zhang,⁸ Z. P. Zhang,³⁰ J. Zhao,⁸ Q. W. Zhao,⁸ Y. F. Zhao,¹³ Y. B. Zhao,⁸ L. Zheng,³⁰
 W. L. Zhong,⁸ L. Zhou,⁸ N. Zhou,³⁰ H. L. Zhuang,⁸ and J. H. Zou⁸

(Daya Bay Collaboration)

¹*Institute of Modern Physics, East China University of Science and Technology, Shanghai*

²*University of Wisconsin, Madison, Wisconsin, USA*

³*Department of Physics, Yale University, New Haven, Connecticut, USA*

⁴*Brookhaven National Laboratory, Upton, New York, USA*

⁵*Department of Physics, National Taiwan University, Taipei*

⁶*National United University, Miaoli*

⁷*Joint Institute for Nuclear Research, Dubna, Moscow Region*

⁸*Institute of High Energy Physics, Beijing*

⁹*Chinese University of Hong Kong, Hong Kong*

¹⁰*Institute of Physics, National Chiao-Tung University, Hsinchu*

¹¹*Shandong University, Jinan*

¹²*Department of Engineering Physics, Tsinghua University, Beijing*

¹³*North China Electric Power University, Beijing*

¹⁴*Shenzhen University, Shenzhen*

¹⁵*Siena College, Loudonville, New York, USA*

¹⁶*Department of Physics, Illinois Institute of Technology, Chicago, Illinois, USA*

¹⁷*Lawrence Berkeley National Laboratory, Berkeley, California, USA*

¹⁸*Department of Physics, University of Illinois at Urbana-Champaign, Urbana, Illinois, USA*

¹⁹*Shanghai Jiao Tong University, Shanghai*

²⁰*Beijing Normal University, Beijing*

²¹*Department of Physics, University of Houston, Houston, Texas, USA*

²²*Center for Neutrino Physics, Virginia Tech, Blacksburg, Virginia, USA*

²³*China Institute of Atomic Energy, Beijing*

²⁴*School of Physics, Nankai University, Tianjin*²⁵*Department of Physics, University of Cincinnati, Cincinnati, Ohio, USA*²⁶*Dongguan University of Technology, Dongguan*²⁷*Department of Physics, University of California, Berkeley, California, USA*²⁸*Department of Physics, The University of Hong Kong, Pokfulam, Hong Kong*²⁹*Charles University, Faculty of Mathematics and Physics, Prague, Czech Republic*³⁰*University of Science and Technology of China, Hefei*³¹*Sun Yat-Sen (Zhongshan) University, Guangzhou*³²*Joseph Henry Laboratories, Princeton University, Princeton, New Jersey, USA*³³*California Institute of Technology, Pasadena, California, USA*³⁴*College of William and Mary, Williamsburg, Virginia, USA*³⁵*Xi'an Jiaotong University, Xi'an*³⁶*Department of Physics, College of Science and Technology, Temple University, Philadelphia, Pennsylvania, USA*³⁷*Instituto de Física, Pontificia Universidad Católica de Chile, Santiago, Chile*³⁸*Nanjing University, Nanjing*³⁹*Department of Physics, Applied Physics, and Astronomy, Rensselaer Polytechnic Institute, Troy, New York, USA*⁴⁰*China General Nuclear Power Group*⁴¹*College of Electronic Science and Engineering, National University of Defense Technology, Changsha*⁴²*Iowa State University, Ames, Iowa, USA*⁴³*Chongqing University, Chongqing*

(Received 13 May 2015; published 11 September 2015)

We report a new measurement of electron antineutrino disappearance using the fully constructed Daya Bay Reactor Neutrino Experiment. The final two of eight antineutrino detectors were installed in the summer of 2012. Including the 404 days of data collected from October 2012 to November 2013 resulted in a total exposure of 6.9×10^5 GW_{th} ton days, a 3.6 times increase over our previous results. Improvements in energy calibration limited variations between detectors to 0.2%. Removal of six ²⁴¹Am-¹³C radioactive calibration sources reduced the background by a factor of 2 for the detectors in the experimental hall furthest from the reactors. Direct prediction of the antineutrino signal in the far detectors based on the measurements in the near detectors explicitly minimized the dependence of the measurement on models of reactor antineutrino emission. The uncertainties in our estimates of $\sin^2 2\theta_{13}$ and $|\Delta m_{ee}^2|$ were halved as a result of these improvements. An analysis of the relative antineutrino rates and energy spectra between detectors gave $\sin^2 2\theta_{13} = 0.084 \pm 0.005$ and $|\Delta m_{ee}^2| = (2.42 \pm 0.11) \times 10^{-3}$ eV² in the three-neutrino framework.

DOI: 10.1103/PhysRevLett.115.111802

PACS numbers: 14.60.Pq, 13.15.+g, 28.50.Hw, 29.40.Mc

Neutrino flavor oscillation due to the mixing angle θ_{13} has been observed using reactor antineutrinos [1–3] and accelerator neutrinos [4,5]. The Daya Bay experiment previously reported the discovery of a nonzero value of $\sin^2 2\theta_{13}$ by observing the disappearance of reactor antineutrinos over kilometer distances [1,6,7], and the first measurement of the effective mass splitting $|\Delta m_{ee}^2|$ [8] via the distortion of the $\bar{\nu}_e$ energy spectrum [9]. Here, we present new results with significant improvements in energy calibration and background reduction. Installation of the final two detectors and a tripling of operation time provided a total exposure of 6.9×10^5 GW_{th} ton days, 3.6 times more than reported in our previous publication [9]. With these improvements the precision of $\sin^2 2\theta_{13}$ was enhanced by a factor of 2 compared to the world's previous best estimate. The precision of $|\Delta m_{ee}^2|$ was equally enhanced, and is now competitive with the precision of $|\Delta m_{32}^2|$ measured via the accelerator neutrino disappearance [10,11].

The Daya Bay experiment started collecting data on 24 December 2011 with six antineutrino detectors (ADs) located in three underground experimental halls (EHs). Three ADs were positioned in two near halls at short distances from six nuclear reactor cores, two ADs in EH1 and one in EH2, and three ADs were positioned in the far hall, EH3. Data taking was paused on 28 July 2012 while two new ADs were installed, one in EH2 and the other in EH3. During the installation, a broad set of calibration sources were deployed into the two ADs of EH1 using automated calibration units [12] and a manual calibration system [13]. Operation of the full experiment with all eight ADs started on 19 October 2012. This Letter presents results based on 404 days of data acquired in the 8-AD period combined with all 217 days of data acquired in the 6-AD period. A blind analysis strategy was implemented by concealing the baselines and target masses of the two new ADs, as well as the operational data of all reactor cores for the new data period.

Each of the three Daya Bay experimental halls hosts functionally identical ADs inside a muon detector system. The latter consists of a two-zone pure water Cherenkov detector, referred to as the inner and outer water shields, covered on top by an array of resistive plate chambers. Each AD consists of three nested cylindrical vessels. The inner vessel is filled with 0.1% gadolinium-doped liquid scintillator (Gd-LS), which constitutes the primary antineutrino target. The vessel surrounding the target is filled with undoped LS, increasing the efficiency of detecting gamma rays produced in the target. The outermost vessel is filled with mineral oil. A total of 192 20-cm photomultiplier tubes (PMTs) are radially positioned in the mineral-oil region of each AD. Further details on the experimental setup are contained in Refs. [14–17]. Reactor antineutrinos are detected via the inverse β -decay (IBD) reaction, $\bar{\nu}_e + p \rightarrow e^+ + n$. The gamma rays (totalling ~ 8 MeV) generated from the neutron capture on Gd with a mean capture time of $\sim 30 \mu\text{s}$ form a delayed signal and enable powerful background suppression. The light from the e^+ gives an estimate of the incident $\bar{\nu}_e$ energy, $E_{\bar{\nu}_e} \approx E_p + \bar{E}_n + 0.78 \text{ MeV}$, where E_p is the prompt energy including the positron kinetic and annihilation energy, and \bar{E}_n is the average neutron recoil energy (~ 10 keV).

Differences in energy responses between detectors directly impacted the estimation of $|\Delta m_{ee}^2|$. PMT gains were calibrated continuously using uncorrelated single electrons emitted by the photocathode. The signals of 0.3% of the PMTs were discarded due to abnormal hit rates or charge distributions. The detector energy scale was calibrated using Am-C neutron sources [18] deployed at the detector center, with the ~ 8 MeV peaks from neutrons captured on Gd aligned across all eight detectors. The time variation and the position dependence of the energy scale was corrected using the 2.506 MeV gamma-ray peak from ^{60}Co calibration sources. The reconstructed energies of various calibration reference points in different ADs are compared in Fig. 1. The spatial distribution of each calibration reference varies, incorporating deviations in spatial response between detectors. Figure 1 presents measurements of ^{68}Ge , ^{60}Co , and Am-C calibration sources when placed at the center of each detector. Neutrons from IBD and muon spallation that were captured on gadolinium, were distributed nearly uniformly throughout the Gd-LS region. Those neutrons that were captured on ^1H , intrinsic α particles from polonium and radon decays, and gammas from ^{40}K and ^{208}Tl decays, were distributed inside and outside of the target volume. All of these events were selected within the Gd-LS region based on their reconstructed vertices. The uncorrelated relative uncertainty of the energy scale is thus determined to be 0.2%. This reduction of 43% compared to the previous publication [9] was enabled by improvements in the correction of position and time dependence, and enhanced the precision of $|\Delta m_{ee}^2|$ by 9%. The reduction was confirmed by an

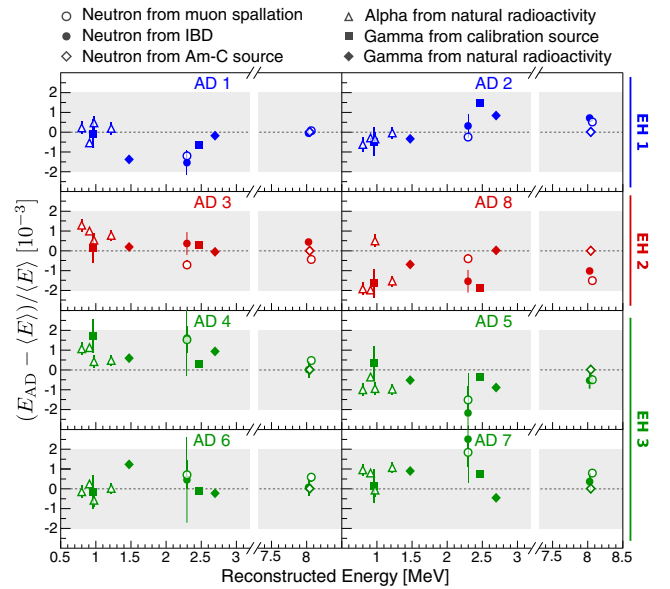


FIG. 1 (color online). Comparison of the reconstructed energy between antineutrino detectors for a variety of calibration references. E_{AD} is the reconstructed energy determined using each AD, and $\langle E \rangle$ is the eight-detector average. Error bars are statistical only, and systematic variations between detectors for all calibration references were $< 0.2\%$. The ~ 8 MeV n -Gd capture gamma peaks from Am-C sources were used to define the energy scale of each detector, and hence show zero deviation.

alternative method which used the n -Gd capture of muon-induced spallation neutrons to calibrate the scale, time dependence, and spatial dependence of the detector energy response.

Nonlinearity in the energy response of an AD originated from two dominant sources: particle-dependent nonlinear light yield of the scintillator and charge-dependent nonlinearity in the PMT readout electronics. Each effect was at the level of 10%. We constructed a semiempirical model that predicted the reconstructed energy for a particle assuming a specific energy deposited in the scintillator. The model contained four parameters: Birks' constant, the relative contribution to the total light yield from Cherenkov radiation, and the amplitude and scale of an exponential correction describing the nonlinear electronics response. This exponential form of the electronics response was motivated by MC and confirmed with an independent FADC measurement.

The nominal parameter values were obtained from an unconstrained χ^2 fit to various AD calibration data sets, comprising twelve gamma lines from both deployed and naturally occurring sources as well as the continuous β -decay spectrum of ^{12}B produced by muon spallation inside the Gd-LS volumes. The nominal positron response derived from the best fit parameters is shown in Fig. 2. The depicted uncertainty band represents other response functions consistent with the fitted calibration data within a

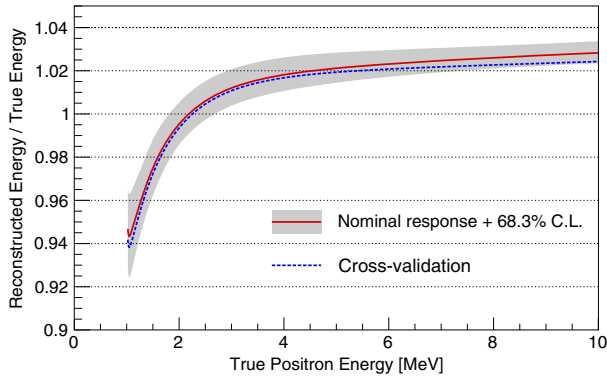


FIG. 2 (color online). Estimated energy response of the detectors to positrons, including both kinetic and annihilation gamma energy (red solid curve). The prominent nonlinearity below 4 MeV was attributed to scintillator light yield (from ionization quenching and Cherenkov light production) and the charge response of the electronics. Gamma rays from both deployed and intrinsic sources as well as spallation ^{12}B β decay determined the model, and provided an envelope of curves consistent with the data within a 68.3% C.L. (grey band). An independent estimate using the beta+gamma energy spectra from ^{212}Bi , ^{214}Bi , ^{208}Tl , as well as the 53-MeV edge in the Michel electron spectrum gave a similar result (blue dashed line), albeit with larger systematic uncertainties.

68.3% C.L. This χ^2 -based approach to obtain the energy response resulted in $< 1\%$ uncertainties of the absolute energy scale above 2 MeV. The uncertainties of the positron response were validated using the 53-MeV cutoff in the Michel electron spectrum from muon decay at rest and the continuous $\beta + \gamma$ spectra from natural bismuth and thallium decays. These improvements added confidence in the characterization of the absolute energy response of the detectors, although they resulted in negligible changes to the measured mixing parameters.

IBD candidates were selected using the same criteria discussed in Ref. [1]. Noise introduced by PMT light emission in the voltage divider, called *flashing*, was efficiently removed using the techniques of Ref. [6]. We required $0.7 \text{ MeV} < E_p < 12.0 \text{ MeV}$, $6.0 \text{ MeV} < E_d < 12.0 \text{ MeV}$, and $1 \mu\text{s} < \Delta t < 200 \mu\text{s}$, where E_d is the delayed energy and $\Delta t = t_d - t_p$ was the time difference between the prompt and delayed signals. In order to suppress cosmogenic products, candidates were rejected if their delayed signal occurred (i) within a $(-2 \mu\text{s}, 600 \mu\text{s})$ time window with respect to an inner water shield or outer water shield trigger with a PMT multiplicity > 12 , (ii) within a $(-2 \mu\text{s}, 1000 \mu\text{s})$ time window with respect to triggers in the same AD with reconstructed energy $> 20 \text{ MeV}$, or (iii) within a $(-2 \mu\text{s}, 1 \text{ s})$ time window with respect to triggers in the same AD with reconstructed energy $> 2.5 \text{ GeV}$. To select only definite signal pairs, we required the signal to have a *multiplicity* of 2: no other $> 0.7 \text{ MeV}$ signal occurred within a $(t_p - 200 \mu\text{s}, t_d + 200 \mu\text{s})$ time window.

Estimates for the five major sources of background for the new data sample are improved with respect to Ref. [9]. The background produced by the three Am-C neutron sources inside the automated calibration units contributed significantly to the total systematic uncertainty of the correlated backgrounds in the 6-AD period. Because of this, two of the three Am-C sources in each AD in EH3 were removed during the 2012 summer installation period. As a result, the average correlated Am-C background rate in the far hall decreased by a factor of 4 in the 8-AD period. As in previous publications [1,9], this rate was determined by monitoring the single-neutron production rate from the Am-C sources. Removal of these Am-C sources had negligible consequences for our calibration.

Energetic, or *fast*, neutrons of cosmogenic origin produced a correlated background for this study. Relaxing the prompt-energy selection to $(0.7\text{--}100) \text{ MeV}$ revealed the fast-neutron background spectrum above 12 MeV. Previously we deduced the rate and spectrum of this background using a linear extrapolation into the IBD prompt signal region. Here we used a background-enhanced data set to improve the estimate. We found 6043 fast-neutron candidates with prompt energy from 0.7 to 100 MeV in the $200 \mu\text{s}$ following cosmogenic signals only detected by the outer water shield or resistive plate chambers. The energy spectrum of these veto-tagged signals was consistent with the spectrum of IBD-like candidate signals above 12 MeV, and was used to estimate the rate and energy spectrum for the fast-neutron background from 0.7 to 12 MeV. The systematic uncertainty was estimated from the difference between this new analysis and the extrapolation method previously employed, and was determined to be half of the estimate reported in Ref. [6].

The methods used in Refs. [1,6] to estimate the backgrounds from the uncorrelated prompt-delayed pairs (i.e., accidentals), the correlated $\beta - n$ decays from cosmogenic ^9Li and ^8He , and the $^{13}\text{C}(\alpha, n)^{16}\text{O}$ reaction, were extended to the current 6 + 8 AD data sample. The decrease in the single-neutron rate from the Am-C sources reduced the average rate of accidentals in the far hall by a factor of 2.7. As a result, the total backgrounds amount to about 3% (2%) of the IBD candidate sample in the far (near) hall(s). The systematic uncertainties in the $^{13}\text{C}(\alpha, n)^{16}\text{O}$ cross section and in the transportation of the α particles were reassessed through a comparison of experimental results and simulation packages, respectively [19]. The estimation of $^9\text{Li}/^8\text{He}$ now dominated the background uncertainty in both the near and far halls. The estimated signal and background rates, as well as the efficiencies of the muon veto, ϵ_μ , and multiplicity selection, ϵ_m , are summarized in Table I.

A detailed treatment of the absolute and relative efficiencies using the first six ADs was reported in Refs. [6,14]. The uncertainties of the absolute efficiencies

TABLE I. Summary of signal and backgrounds. Rates are corrected for the muon veto and multiplicity selection efficiencies $\epsilon_\mu \cdot \epsilon_m$. The measured ratio of the IBD rates in AD1 and AD2 (AD3 and AD8 in the 8-AD period) was 0.981 ± 0.004 (1.019 ± 0.004) while the expected ratio was 0.982 (1.012).

| | EH1 | | EH2 | | EH3 | | | |
|--|-------------------|-------------------|-------------------|-------------------|------------------|------------------|------------------|------------------|
| | AD1 | AD2 | AD3 | AD8 | AD4 | AD5 | AD6 | AD7 |
| IBD candidates | 304 459 | 309 354 | 287 098 | 190 046 | 40 956 | 41 203 | 40 677 | 27 419 |
| DAQ live time (days) | 565.436 | 565.436 | 568.03 | 378.407 | 562.451 | 562.451 | 562.451 | 372.685 |
| ϵ_μ | 0.8248 | 0.8218 | 0.8575 | 0.8577 | 0.9811 | 0.9811 | 0.9808 | 0.9811 |
| ϵ_m | 0.9744 | 0.9748 | 0.9758 | 0.9756 | 0.9756 | 0.9754 | 0.9751 | 0.9758 |
| Accidentals (per day) | 8.92 ± 0.09 | 8.94 ± 0.09 | 6.76 ± 0.07 | 6.86 ± 0.07 | 1.70 ± 0.02 | 1.59 ± 0.02 | 1.57 ± 0.02 | 1.26 ± 0.01 |
| Fast neutron (per AD per day) | 0.78 ± 0.12 | | 0.54 ± 0.19 | | 0.05 ± 0.01 | | | |
| ${}^9\text{Li}/{}^8\text{He}$ (per AD per day) | 2.8 ± 1.5 | | 1.7 ± 0.9 | | 0.27 ± 0.14 | | | |
| Am-C correlated 6-AD (per day) | 0.27 ± 0.12 | 0.25 ± 0.11 | 0.27 ± 0.12 | | 0.22 ± 0.10 | 0.21 ± 0.10 | 0.21 ± 0.09 | |
| Am-C correlated 8-AD (per day) | 0.20 ± 0.09 | 0.21 ± 0.10 | 0.18 ± 0.08 | 0.22 ± 0.10 | 0.06 ± 0.03 | 0.04 ± 0.02 | 0.04 ± 0.02 | 0.07 ± 0.03 |
| ${}^{13}\text{C}(\alpha, n){}^{16}\text{O}$ (per day) | 0.08 ± 0.04 | 0.07 ± 0.04 | 0.05 ± 0.03 | 0.07 ± 0.04 | 0.05 ± 0.03 | 0.05 ± 0.03 | 0.05 ± 0.03 | 0.05 ± 0.03 |
| IBD rate (per day) | 657.18 ± 1.94 | 670.14 ± 1.95 | 594.78 ± 1.46 | 590.81 ± 1.66 | 73.90 ± 0.41 | 74.49 ± 0.41 | 73.58 ± 0.40 | 75.15 ± 0.49 |

are correlated among the ADs and thus play a negligible role in the relative measurement of $\bar{\nu}_e$ disappearance. The performance of the two new ADs was found to be consistent with the other detectors. Estimates of two prominent uncorrelated uncertainties, the delayed-energy selection efficiency and the fraction of neutrons captured on Gd, were confirmed for all eight ADs using improved energy reconstruction and increased statistics.

Oscillation was measured using the L/E -dependent disappearance of $\bar{\nu}_e$, as given by the survival probability

$$P = 1 - \cos^4\theta_{13}\sin^2 2\theta_{12}\sin^2 \frac{1.267\Delta m_{21}^2 L}{E} - \sin^2 2\theta_{13}\sin^2 \frac{1.267\Delta m_{ee}^2 L}{E}. \quad (1)$$

Here E is the energy in MeV of the $\bar{\nu}_e$, L is the distance in meters from its production point, θ_{12} is the solar mixing angle, and $\Delta m_{21}^2 = m_2^2 - m_1^2$ is the mass-squared difference of the first two neutrino mass eigenstates in eV^2 .

Recent precise measurements of the IBD positron energy spectrum disagree with models of reactor $\bar{\nu}_e$ emission [3,20–22]. The characteristics of the signals in this energy range are consistent with reactor antineutrino emission, and disfavor background or detector response as possible origins for the discrepancy. Reference [20] presents the evidence in detail and provide the necessary data to allow detailed comparison of our measurement with existing and future models. Given these discrepancies between

measurements and models, here we present a technique for predicting the signal in the far hall based on measurements obtained in the near halls, with minimal dependence on models of the reactor antineutrinos. In our previous measurements [9], model dependence was limited by allowing variation of the predicted $\bar{\nu}_e$ flux within model uncertainties, while the technique here provides an explicit demonstration of the negligible model dependence. A χ^2 was defined as

$$\chi^2 = \sum_{i,j} (N_j^f - w_j N_j^n) (V^{-1})_{ij} (N_i^f - w_i N_i^n), \quad (2)$$

where N_i is the observed number of events after background subtraction in the i th bin of reconstructed positron energy E^{rec} . The superscript $f(n)$ denotes a far (near) detector. The symbol V represents a covariance matrix that includes known systematic and statistical uncertainties. The quantity w_i is a weight that accounts for the differences between near and far measurements. For the case of a single reactor, the weight w_i can be simply calculated from the ratios of detector mass, distance to the reactor, efficiency, and antineutrino oscillation probability, as given by the relation:

$$w_i^{\text{SR}} = \frac{N_i^f}{N_i^n} = \left(\frac{T^f}{T^n}\right) \left(\frac{\epsilon^f}{\epsilon^n}\right) \left(\frac{L^n}{L^f}\right)^2 \left(\frac{P_i^f}{P_i^n}\right) \left(\frac{\phi}{\phi}\right). \quad (3)$$

Here T is the number of target protons, ϵ is the efficiency, and L is the distance to the reactor for a given detector. P_i is

the oscillation probability for the i th reconstructed energy bin and ϕ the reactor antineutrino flux (which cancels from w_i). With P_i calculated in reconstructed positron energy, the detector response introduces small ($< 0.2\%$ above 2 MeV) calculable deviations from Eq. (1).

For multiple reactor cores, the weight w_i was modified:

$$w_i = \frac{N_i^f}{N_i^n} = \left(\frac{T^f}{T^n}\right) \left(\frac{\epsilon^f}{\epsilon^n}\right) \sum_j \mathcal{P}(E_j^{\text{true}} | E_i^{\text{rec}}) r_j. \quad (4)$$

The probability distribution $\mathcal{P}(E_j^{\text{true}} | E_i^{\text{rec}})$ accounts for the energy transfer from the $\bar{\nu}_e$ to the e^+ and imperfections in the detector energy response (loss in nonactive elements, nonlinearity, and resolution). The extrapolation factor r_j was calculated as

$$r_j = \frac{\sum_k^{\text{cores}} P(E_j^{\text{true}}, L_k^f) \phi_{jk} / (L_k^f)^2}{\sum_k^{\text{cores}} P(E_j^{\text{true}}, L_k^n) \phi_{jk} / (L_k^n)^2}, \quad (5)$$

where P is given by Eq. (1), $L_k^{f(n)}$ is the distance between a far (near) detector and core k , and ϕ_{jk} is the predicted antineutrino flux from core k for the j th true energy bin. In the single-reactor core case, the antineutrino flux ϕ cancels in the expression for r_j and Eq. (4) reduces to Eq. (3). Although the cancellation is not exact for multiple cores, the impact of the uncertainty in reactor antineutrino flux was found to be $\leq 0.1\%$.

The covariance matrix element V_{ij} was the sum of a statistical term, calculated analytically, and a systematic term determined by Monte Carlo calculation using

$$V_{ij} = \frac{1}{N} \sum (S_i^f - w_i S_i^n)(S_j^f - w_j S_j^n). \quad (6)$$

Here, N is the number of simulated experiments generated with energy spectra S , including systematic variations of detector response, $\bar{\nu}_e$ flux, and background. The choice of reactor antineutrino model [22–28] in calculating the covariance had negligible ($< 0.2\%$) impact on the determination of the oscillation parameters.

Without loss of sensitivity, we summed the IBD signal candidates of the ADs within the same hall, accounting for small differences of target mass, detection efficiency, background, and baseline. We considered the 6-AD and 8-AD periods separately in order to properly handle correlations in reactor antineutrino flux, detector exposure, and background. This means that i and j in the above equations ran over the 37 reconstructed energy bins for the two near versus far combinations and for the two periods considered ($37 \times 2 \times 2 = 148$). More details of this method are described in Ref. [29].

Using this method, we found $\sin^2 2\theta_{13} = 0.084 \pm 0.005$ and $|\Delta m_{ee}^2| = (2.42 \pm 0.11) \times 10^{-3} \text{ eV}^2$, with $\chi^2/\text{NDF} = 134.6/146$ (see the Supplemental Material [30]). While we

use $\sin^2 2\theta_{12} = 0.857 \pm 0.024$ and $\Delta m_{21}^2 = (7.50 \pm 0.20) \times 10^{-5} \text{ eV}^2$ from Ref. [31], our result was largely independent of these values. Consistent results were obtained when our previous methods [1,9] were applied to this larger data set. Under the normal (inverted) hierarchy assumption, $|\Delta m_{ee}^2|$ yields $\Delta m_{32}^2 = (2.37 \pm 0.11) \times 10^{-3} \text{ eV}^2$ ($\Delta m_{32}^2 = -(2.47 \pm 0.11) \times 10^{-3} \text{ eV}^2$). This result was consistent with and of comparable precision to measurements obtained from accelerator ν_μ and $\bar{\nu}_\mu$ disappearance [10,11]. Using only the relative rates between the detectors and Δm_{32}^2 from Ref. [10] we found $\sin^2 2\theta_{13} = 0.085 \pm 0.006$, with $\chi^2/\text{NDF} = 1.37/3$.

The reconstructed positron energy spectrum observed in the far site is compared in Fig. 3 with the expectation based on the near-site measurements. The 68.3%, 95.5%, and 99.7% C.L. allowed regions in the $|\Delta m_{ee}^2| - \sin^2 2\theta_{13}$ plane are shown in Fig. 4. The spectral shape from all experimental halls is compared in Fig. 5 to the electron antineutrino survival probability assuming our best estimates of the oscillation parameters. The total uncertainties of both $\sin^2 2\theta_{13}$ and $|\Delta m_{ee}^2|$ are dominated by statistics. The most significant systematic uncertainties for $\sin^2 2\theta_{13}$ are due to the relative detector efficiency, reactor power, relative energy scale, and ${}^9\text{Li}/{}^8\text{He}$ background. The

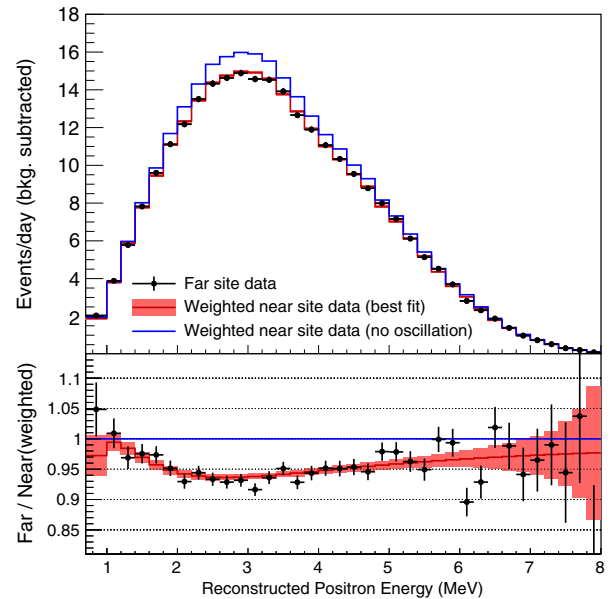


FIG. 3 (color online). Upper: Background-subtracted reconstructed positron energy spectrum observed in the far site (black points), as well as the expectation derived from the near sites excluding (blue line) or including (red line) our best estimate of oscillation. The spectra were efficiency corrected and normalized to one day of live time. Lower: Ratio of the spectra to the no-oscillation case. The error bars show the statistical uncertainty of the far site data. The shaded area includes the systematic and statistical uncertainties from the near-site measurements.

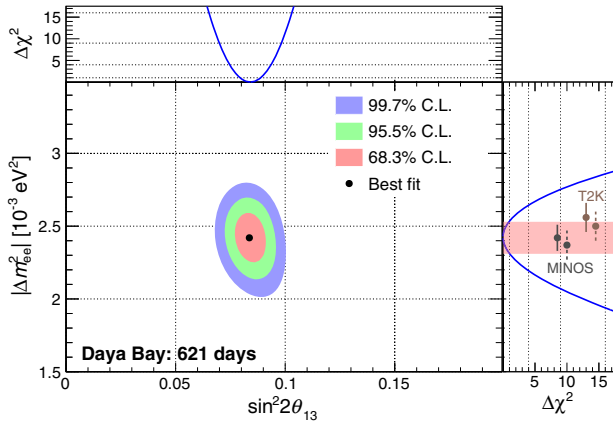


FIG. 4 (color online). Regions in the $|\Delta m_{ee}^2| - \sin^2 2\theta_{13}$ plane allowed at the 68.3%, 95.5%, and 99.7% confidence levels by the near-far comparison of $\bar{\nu}_e$ rate and energy spectra. The best estimates were $\sin^2 2\theta_{13} = 0.084 \pm 0.005$ and $|\Delta m_{ee}^2| = (2.42 \pm 0.11) \times 10^{-3} \text{ eV}^2$ (black point). The adjoining panels show the dependence of $\Delta\chi^2$ on $\sin^2 2\theta_{13}$ (top) and $|\Delta m_{ee}^2|$ (right). The $|\Delta m_{ee}^2|$ allowed region (shaded band, 68.3% C.L.) was consistent with measurements of $|\Delta m_{32}^2|$ using muon disappearance by the MINOS [10] and T2K [11] experiments, converted to $|\Delta m_{ee}^2|$ assuming the normal (solid) and inverted (dashed) mass hierarchy.

systematic uncertainty in $|\Delta m_{ee}^2|$ is dominated by uncertainty in the relative energy scale.

In summary, enhanced measurements of $\sin^2 2\theta_{13}$ and $|\Delta m_{ee}^2|$ have been obtained by studying the energy-dependent disappearance of the electron antineutrino interactions recorded in a $6.9 \times 10^5 \text{ GW}_{\text{th}}$ ton days exposure. Improvements in calibration, background estimation, as

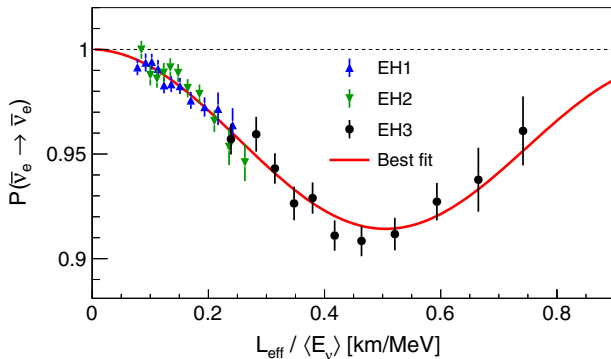


FIG. 5 (color online). Electron antineutrino survival probability versus effective propagation distance L_{eff} divided by the average antineutrino energy $\langle E_{\nu} \rangle$. The data points represent the ratios of the observed antineutrino spectra to the expectation assuming no oscillation. The solid line represents the expectation using the best estimates of $\sin^2 2\theta_{13}$ and $|\Delta m_{ee}^2|$. The error bars are statistical only. $\langle E_{\nu} \rangle$ was calculated for each bin using the estimated detector response, and L_{eff} was obtained by equating the actual flux to an effective antineutrino flux using a single baseline.

well as increased statistics allow this study to provide the most precise estimates to date of the neutrino mass and mixing parameters $|\Delta m_{ee}^2|$ and $\sin^2 2\theta_{13}$.

Daya Bay is supported in part by the Ministry of Science and Technology of China, the U.S. Department of Energy, the Chinese Academy of Sciences, the CAS Center for Excellence in Particle Physics, the National Natural Science Foundation of China, the Guangdong provincial government, the Shenzhen municipal government, the China General Nuclear Power Group, Key Laboratory of Particle and Radiation Imaging (Tsinghua University), the Ministry of Education, Key Laboratory of Particle Physics and Particle Irradiation (Shandong University), the Ministry of Education, Shanghai Laboratory for Particle Physics and Cosmology, the Research Grants Council of the Hong Kong Special Administrative Region of China, the University Development Fund of The University of Hong Kong, the MOE program for Research of Excellence at National Taiwan University, National Chiao-Tung University, and NSC fund support from Taiwan, the U.S. National Science Foundation, the Alfred P. Sloan Foundation, the Ministry of Education, Youth, and Sports of the Czech Republic, the Joint Institute of Nuclear Research in Dubna, Russia, the NSFC-RFBR joint research program, the National Commission of Scientific and Technological Research of Chile, and the Tsinghua University Initiative Scientific Research Program. We acknowledge Yellow River Engineering Consulting Co., Ltd., and China Railway 15th Bureau Group Co., Ltd., for building the underground laboratory. We are grateful for the ongoing cooperation from the China General Nuclear Power Group and China Light and Power Company.

- [1] F. P. An *et al.* (Daya Bay Collaboration), *Phys. Rev. Lett.* **108**, 171803 (2012).
- [2] J. Ahn *et al.* (RENO Collaboration), *Phys. Rev. Lett.* **108**, 191802 (2012).
- [3] Y. Abe *et al.* (Double Chooz Collaboration), *J. High Energy Phys.* **10** (2014) 86.
- [4] K. Abe *et al.* (T2K Collaboration), *Phys. Rev. Lett.* **112**, 061802 (2014).
- [5] P. Adamson *et al.* (MINOS Collaboration), *Phys. Rev. Lett.* **110**, 171801 (2013).
- [6] F. P. An *et al.* (Daya Bay Collaboration), *Chin. Phys. C* **37**, 011001 (2013).
- [7] F. P. An *et al.* (Daya Bay Collaboration), *Phys. Rev. D* **90**, 071101 (2014).
- [8] Δm_{ee}^2 is an effective mass splitting that can be obtained by replacing $\cos^2 \theta_{12} \sin^2 \Delta_{31} + \sin^2 \theta_{12} \sin^2 \Delta_{32}$ with $\sin^2 \Delta_{ee}$, where $\Delta_{ji} \equiv 1.267 \Delta m_{ji}^2 (\text{eV}^2) [L (\text{m}) / E (\text{MeV})]$, and Δm_{ji}^2 is the difference between the mass-squares of the mass eigenstates ν_j and ν_i . To estimate the values of Δm_{31}^2 and Δm_{32}^2 from the measured value of Δm_{ee}^2 , See Supplemental Material at <http://link.aps.org/supplemental/10.1103/PhysRevLett.115.111802>.

- [9] F. P. An *et al.* (Daya Bay Collaboration), *Phys. Rev. Lett.* **112**, 061801 (2014).
- [10] P. Adamson *et al.* (MINOS Collaboration), *Phys. Rev. Lett.* **112**, 191801 (2014).
- [11] K. Abe *et al.* (T2K Collaboration), *Phys. Rev. Lett.* **112**, 181801 (2014).
- [12] J. L. Liu, B. Cai, R. Carr, D. A. Dwyer, W. Q. Gu, G. S. Li, X. Qian, R. D. McKeown, R. H. M. Tsang, W. Wang *et al.*, *Nucl. Instrum. Methods Phys. Res., Sect. A* **750**, 19 (2014).
- [13] H. X. Huang, X. C. Ruan, J. Ren, C. J. Fan, Y. N. Chen, Y. L. Lv, Z. H. Wang, Z. Y. Zhou, L. Hou, B. Xin *et al.*, *J. Instrum.* **8**, P09013 (2013).
- [14] F. P. An *et al.* (Daya Bay Collaboration), *Nucl. Instrum. Methods Phys. Res., Sect. A* **685**, 78 (2012).
- [15] F. P. An *et al.* (Daya Bay Collaboration), *Nucl. Instrum. Methods Phys. Res., Sect. A* **773**, 8 (2015).
- [16] F. P. An *et al.* (Daya Bay Collaboration), [arXiv:1508.03943](https://arxiv.org/abs/1508.03943).
- [17] F. P. An *et al.* (Daya Bay Collaboration), [arXiv:hep-ex/0701029](https://arxiv.org/abs/hep-ex/0701029).
- [18] J. Liu, R. Carr, D. A. Dwyer, W. Q. Gu, G. S. Li, R. D. McKeown, X. Qian, R. H. M. Tsang, F. F. Wu, and C. Zhang, *Nucl. Instrum. Methods Phys. Res., Sect. A* **797**, 260 (2015).
- [19] J. Zhao, Z. Y. Yu, J. L. Liu, X. B. Li, F. H. Zhang, and D. M. Xia, *Chin. Phys. C* **38**, 116201 (2014).
- [20] F. P. An *et al.* (Daya Bay Collaboration), [arXiv:1508.04233](https://arxiv.org/abs/1508.04233).
- [21] S. Seo (RENO Collaboration), in *Neutrino2014: The XXVI International Conference on Neutrino Physics and Astrophysics*, Boston, 2014 (unpublished).
- [22] D. A. Dwyer and T. J. Langford, *Phys. Rev. Lett.* **114**, 012502 (2015).
- [23] K. Schreckenbach, G. Colvin, W. Gelletly, and F. von Feilitzsch, *Phys. Lett. B* **160**, 325 (1985).
- [24] A. A. Hahn, K. Schreckenbach, W. Gelletly, F. von Feilitzsch, G. Colvin, and B. Krusche, *Phys. Lett. B* **218**, 365 (1989).
- [25] F. von Feilitzsch, A. Hahn, and K. Schreckenbach, *Phys. Lett. B* **118**, 162 (1982).
- [26] P. Vogel, G. K. Schenter, F. M. Mann, and R. E. Schenter, *Phys. Rev. C* **24**, 1543 (1981).
- [27] P. Huber, *Phys. Rev. C* **84**, 024617 (2011).
- [28] Th. A. Mueller, D. Lhuillier, M. Fallot, A. Letourneau, S. Cormon, M. Fechner, L. Giot, T. Lasserre, J. Martino, G. Mention *et al.*, *Phys. Rev. C* **83**, 054615 (2011).
- [29] Y. Nakajima, J. P. Ochoa-Ricoux, and H. L. H. Wong (to be published).
- [30] See Supplemental Material at <http://link.aps.org/supplemental/10.1103/PhysRevLett.115.111802> for a table of $\chi^2 - \chi_{\min}^2$ as a function of $(\sin^2 2\theta_{13}, |\Delta m_{ee}^2|)$.
- [31] J. Beringer *et al.* (Particle Data Group), *Phys. Rev. D* **86**, 010001 (2012), see Sec. 13.